Predictive Models and Detection Methods Applicable in Water Detection Framework for Industrial Electric Arc Furnaces

Hamzah Alshawarghi , Ali Elkamel , Behzad Moshiri , Farzad Hourfar

PII: S0098-1354(18)31352-8
DOI: https://doi.org/10.1016/j.compchemeng.2019.06.005
Reference: CACE 6480

To appear in: *Computers and Chemical Engineering*

Received date: 25 December 2018
Revised date: 14 May 2019
Accepted date: 5 June 2019

Please cite this article as: Hamzah Alshawarghi , Ali Elkamel , Behzad Moshiri , Farzad Hourfar , Predictive Models and Detection Methods Applicable in Water Detection Framework for Industrial Electric Arc Furnaces, *Computers and Chemical Engineering* (2019), doi: https://doi.org/10.1016/j.compchemeng.2019.06.005

Predictive Models and Detection Methods Applicable in Water Detection Framework for Industrial Electric Arc Furnaces

Hamzah Alshawarghi [a], Ali Elkamel [a, b 1], Behzad Moshiri [c], Farzad Hourfar [c]

[a] Department of Chemical Engineering, University of Waterloo, Waterloo, Ontario, Canada

[b] Department of Chemical Engineering, The Petroleum Institute, Khalifa University of Science & Technology, Abu Dhabi, UAE

[c] Control & Intelligent Processing Center of Excellence (CIPCE), School of Electrical & Computer Engineering, University of Tehran, Tehran, Iran

Abstract

This paper introduces the development of empirical predictive models and detection methods that are incorporated into a water detection framework for an industrial steelmaking electric arc furnace (EAF). The predictive models investigated in this work are designed based on different techniques such as statistical fingerprinting, artificial neural network (ANN), and multiway projection to latent structures (MPLS). Robustness issues related to each method are discussed and performance comparisons have been done for the presented techniques. Furthermore, model fusion theory has been applied to improve the prediction accuracy of the developed models' defined output- the value of off-gas water vapor- which is known as one the most vital variables to guarantee a safe and reliable operation. Finally based on the proposed predictive models, a water leak detection methodology is introduced and implemented on an industrial AC EAF and a comprehensive discussion has been done to evaluate the performance

[1] Corresponding Author (aelkamel@uwaterloo.ca).

of the developed algorithm. To this aim, two fault detection methods have been applied. Fault detection method #1 has been designed using statistical fingerprinting technique, while the other one has been developed based on machine learning-based models and also fusion of the models' outputs.

Keywords: EAF water detection framework, Fingerprinting, Artificial Neural Network (ANN), Multiway Projection to Latent Structures (MPLS), Model Fusion, Fault Detection

1 Introduction

Electric Arc Furnaces (EAFs) are used in the steel industry to produce liquid steel. The feed iron material is melted using electrical and chemical energy in the furnace, and the molten steel chemistry is adjusted to obtain the desired grade specifications. The electric arc furnace is a batch process producing batches of liquid steel known as heats. The electrical energy is added to the furnace through electrodes in the form of electric arc, and the chemical energy is added using a fuel source such as methane, oxygen, and carbon. Typical heats in electric arc furnaces vary greatly because of the different operating conditions. However; most of modern operations aim for a heat cycle less than one hour with electric energy consumption in the range of 380-400 kWh/tonne (Jones et al., 2005).

The electric arc furnace heat sequence consists of the following steps: grade selection, bucket preparation, furnace charging, melting, refining, de-slagging, tapping, and furnace turn-around. The heat steps are discussed in more details by (Fruehan, 1998) and (Jones et al, 2005). The primary raw material used for EAF steelmaking is scrap. Scrap varies in chemical composition and it can contain contaminants such as copper that are undesirable for steelmaking. Steelmaking

facilities that produce higher quality products typically use cleaner iron raw material such as Direct Reduction Iron (DRI), which contains low contaminants.

The first step in a heat is to select the steel grade to be produced; next the scrap quality in the bucket is prepared based on the chosen steel grade to ensure that the grade specifications are met at the end of the heat. The second step is to prepare the scrap bucket. The operator layers the scrap in the bucket according to the size and density of the scrap so that the molten steel is formed faster in the furnace. Moreover, lime and carbon can be added to the bucket with the scrap, or they can be injected into the furnace during the heat. The third step is charging the buckets into the furnace, where the roof and the electrode are raised and moved to the sides to allow the crane to charge the scrap bucket into the furnace. Once the operator finishes charging the scrap, the roof and the electrodes swing back and are lowered to start the electrical arc. If the steelmaking facility uses DRI as iron raw material, then typically DRI is continuously fed through the roof of the furnace during the heat. Modern scrap furnaces aim to operate with two or three charge buckets of scrap, because charging is a dead-time where the furnace is not melting, and also there are radiation losses every time the roof opens.

The fourth step is melting which is the core in EAF operations. Modern EAF designs maximize the melting efficiency of the furnace. Melting is accomplished by supplying electrical energy and chemical energy to the furnace. The electrodes are used in the furnace to supply the electrical energy, where in the beginning of the heat, an intermediate voltage tap is used to allow the electrodes to bore into the scrap. Once enough liquid is formed, then a high voltage tap (Long arc) is selected. A long arc allows more energy to be transferred to the scrap through the radiation of the arc than a short arc. Moreover, at the start of melting the arc is unstable. However; once a molten bath forms, the arc becomes stable and the energy input to the steel bath

increases. The charging process is repeated once enough scrap has been melted to accommodate the subsequent bucket. Once the final scrap bucket is charged and melted, the formation of a foamy slag is critical to bury the arc and protect the furnace sidewalls. The foamy slag is formed by injecting carbon and oxygen which forms carbon monoxide bubbles in the slag. Moreover, once all scrap is melted and flat bath conditions are reached, a shorter electrical arc is used to minimize exposing the furnace sidewalls to the arc radiations.

The refining phase of the heat starts when flat bath conditions are reached. The operator's first objective is to inject oxygen to lower bath carbon, aluminum, silicon, and manganese contents to the desired level for tapping, where oxygen reacts with these elements to form metallic oxides that float out of the steel bath and into the slag layer. The operator's second objective during refining is to increase bath temperature using electrical energy to the desired tapping temperature. The de-slagging phase is then carried out to remove the slag that accumulated in the furnace during refining. Once the desired steel grade composition and temperature are achieved in the furnace, tapping is carried out which is to discharge the steel into a ladle to be transferred to the next operation. The last step of the heat is the furnace turn-around which is the period that follows tapping during which the operator inspects the furnace interior for any refractory damages or water leaks from the panels.

In modern EAFs, the cooling water system is an essential part of the furnace used to cool the roof and the sidewall panels. Water leaks typically occur from those panels. Usually, the water flows at a continuous rate of approximately 165-185 liters/minute/m^2 of cooled area. The total cooling water flowrate requirement for a typical EAF ranges between 16,650 and 23,850 liters/ minute (Quiroga, 2013). Due to the high flowrate of water in the furnace panels, a small leak in water cooled panels can quickly result in significant amounts of water in the furnace.

Furthermore, if this water leaks into the EAF and comes in contact with molten steel, there is the potential for a severe explosion. Consequently, water leaks in the EAF present a serious and dangerous situation. Personnel safety, damaged equipment, and production losses are possible effects of water leaks in the furnace.

Generally, water leak explosions result in fatalities. The frequency of water leak accidents may vary from once every few months to once every few years. Reasons for the frequency difference include safety standards implemented in the melt-shop and technologies such as flow meters installed on the water cooled panels. The benefits for accurately detecting water leaks can minimize the risk of such furnace explosions.

During the last decade, there have been significant advances in the EAF technology that have focused on increasing productivity leading to lower cost steel production. However, due to the severe consequences of furnace explosions caused by water leaks inside the furnace in the recent years, there has been a growing demand for safety issues.

Currently, EAF operators use the flow of water inside the EAF water cooled panels to provide an indication if there is water leak from the panels inside the furnace. However, the measurement noise limits its effectiveness to larger water leaks in the range of 90-180 liters/min (Zuliani et al., 2014). In addition, there are off-gas analyzer system suppliers that have developed systems to measure the off-gas water vapor (e.g. Grieshaber, K. and F. Martinez, 2015), and by monitoring the changes due to unexpected additional water sources, the leaks can be detected. However, due to the high variability in the EAF process, it may be insufficient to use only the measured variables to detect the water leak occurrence.

Based on the above explanations, since water leaks have historically posed serious safety concerns for every steel plant, there is industrial and academic needs to explore for effective water leak detection methodologies in EAFs. So, to respond to this crucial issue, in this paper a framework has been developed to distinguish between normal and abnormal (Faulty) operational condition in an industrial EAF. It has been also demonstrated in the following sections that by applying model fusion technique, the estimation quality of off-gas water vapor is much better compared with just using a single machine learning-based model as a humidity predictor.

2 Fault Detection Approaches

In General, fault detection methods can be classified as model-based, and data-driven techniques. Model-based methods rely on fundamental understanding of the process where data-driven approaches rely on historical data. Model-based fault detection methods have been around for many years but their contribution to the industrial practice is limited due to the cost and time required to develop accurate models for complex industrial processes. On the other hand, the data-driven approaches generally require less time and lower cost to be developed. Empirical methods commonly used for data-driven fault detection approaches include artificial neural network (Chetouani, 2008), multiway principal component analysis (Nomikos and MacGregor (1994)), and Bayesian approach (Yu, 2012). Furthermore, Freeman et al. (2013) compared and applied both approaches to a small unmanned aerial vehicles (UAV) platform.

MacGregor and Nomikos (1994) developed a multivariate statistical method for monitoring batch processes where the only required information was good historical batches. The applied empirical method was a multiway principal component analysis (MPCA). MPCA was used to extract the information from the multivariate dimensions and to project them onto lower-dimensional space, defined by principal components. The method used by the authors to

calculate the principal component was the NIPALS algorithm. Moreover, due to the three-dimensional array nature of the batch data (batches, measurements, and time), the authors unfolded the three-dimensional array to a two-dimensional array, and then they built the MPCA model. The authors determined that three principal components were necessary to precisely describe the normal operation of a batch. Monitoring plots generated by the MPCA method were the score plots and loading plots for the latent variables of the MPCA model. These plots included control limits corresponding to 95% and 99% confidence regions, calculated based on the reference heats. The MPCA monitoring plots were used online to monitor the progress of a new batch in real-time. The MPCA method was based on the concept that future behavior of a process was monitored by comparing it against the past in which the process was performing well. Two fundamental assumptions were necessary for the MPCA method to work properly. The first assumption was: "The reference database is representative of the process operation, and hence if something changes in the process, then a new MPCA model must be built on the new batches. The second assumption was: "The fault event must be observable from the collected measurements in order to be detected by the MPCA model.

Chetouani (2008) developed an artificial neural network (ANN) approach for real-time detection of faults. This approach combined ANN and CUSUM statistical test for fault detection. The developed ANN model was a one layer perceptron network, and the process used in that work was a reactor-exchanger setup. The training algorithm used to develop the ANN model was the back-propagation training function for feed-forward networks using momentum and adaptive learning technique. The author utilized the CUSUM statistical test for fault detection, where that test was performed as a cumulative sum test. The jumps in the mean occur at unknown time

instants in the designed experiment. The considered reactor-exchanger to test this method was a glass-jacketed reactor with a tangential input for heat transfer fluid.

Sheibat-Othman et al. (2014) proposed a hybrid data/model-based approach for fault detection for chemical reactions. Two stirred tank jacketed chemical reactors were used. The reactor was equipped with temperature probes and the feed mixture was put on a balance to calculate the feed flowrate. Temperature sensor faults and actuator faults (capacity for heating and cooling) were used to investigate the proposed hybrid methodology. The process model developed for the system was a heat balance of a semi-continuous stirred tank reactor and its jacket. The authors used two class support vectors machine (SVM) for the data driven model. Furthermore, it was found that it would require a great number of data to train the SVM model, because the reactions in the reactor were highly nonlinear. Therefore, a simplified process model was considered as a starting point to develop an observer for fault isolation. In addition, information from the SVM model was used to correct the simplified process model when no faults were detected. It was also found out that the single SVM model was sufficient to detect faults, if the process dynamics were totally linear.

Freeman et al. (2013) designed and applied a model-based residual generation and data driven fault detection approaches to a small unmanned aerial vehicles (UAV) platform. The electric powered airplane had a 1.3 meters wingspan and a weight of 1.3 kg. The model based fault detection strategy used linear filtering methods to reject faults. Raw flight data was used to develop the data driven algorithm without knowledge of system dynamics. An H∞ filter was constructed to detect aileron faults. A data driven detector was developed by processing the control error signals logged from the flight data and consequently creating an error score related to the probability of a fault. Both approaches successfully detected different aileron faults during

maneuvers and in the presence of environmental disturbances. However, the performance of the data driven detector suffered in the linear simulations with high model uncertainty and was not always successful to detect all the existing faults. In that case, the system knowledge which was built in the model-based framework allowed for better performance.

3 Statistical Fingerprinting

3.1 Statistical Fingerprinting Method

There are few EAF operations where the process is well controlled, and hence there is a minimal variability in the process. In these operations, scrap quality does not vary significantly, the operator uses the same chemical program, and there is limited weather variation. These conditions allow for the off-gas water vapor to behave similarly from heat to heat. Consequently, in these EAF operations, the off-gas measurement of water vapor can provide adequate indication and metrics to distinguish between normal and abnormal levels of water vapor in the EAF. Although the off-gas water vapor concentration varies throughout the melting and refining phases of the heat, the statistical fingerprinting method has been developed to characterize the off-gas water vapor over a number of heats with similar operating conditions such as number of charges, scrap recipe, and chemical program (Zuliani et al., 2014). For example, Figure 1 shows the typical off-gas water vapor trend for the first melting charge on a kWh basis for several heats with similar operating conditions. Figure 1 also shows a baseline average curve for the off-gas water vapor. The heat time shown in Figure 1 is kWh which is a typical energy clock used by melt-shops to pace the heat.

The first step in this method is to start with a set of heats with similar operating conditions. This set is used as a training set to calculate the fingerprints thresholds, which is used

on future heats to detect for potential water leaks. The second step in this method is to manually divide the charge time into bins of similar dynamics. This step enables the off-gas water vapor to be characterized across multiple heats in a single bin. The third step is to compute a fingerprint threshold value in each bin that represents an upper limit. The used statistic indices in the fingerprinting method are the median and median absolute deviation (MAD). The median is a measure of sample location and is computed by sorting the data and taking the middle value. The median is a robust estimator of the sample location and MAD is a robust measure of variation (Dunn, 2014). However, the median and the MAD become unbounded if half of the data is replaced with outliers. MAD is computed by Equation 1:

$$\text{MAD}\,(x_i) = c \times \text{median}\,(\text{abs}\,(x_i - \text{median}\,(x_i))) \quad (1)$$

$$c = 1.4826$$

The constant c makes the MAD consistent with the standard deviation when the observations x_i are normally distributed. The fingerprint threshold is calculated using Equation 2:

$$\text{Fingerprint Upper Limit} = \text{Median} + 2 \times \text{MAD} \quad (2)$$

The fingerprint thresholds provide the basis to detect abnormal water vapor by comparing the measured water vapor of the current heat to the fingerprint threshold value in each bin. Specifically, if the value of the measured water vapor of the current heat is higher than the fingerprint threshold value, then there is a statistical condition which is equivalent to existence of abnormal water vapor in the EAF. Figure 1 depicts an example for a heat (in red color) with water vapor significantly above the fingerprint and also for an extended time. It can be easily observed that all other curves (in different colors) are below the fingerprint threshold value. As a result, other heats are assumed to be in normal condition, without any abnormality on water vapor in EAF.

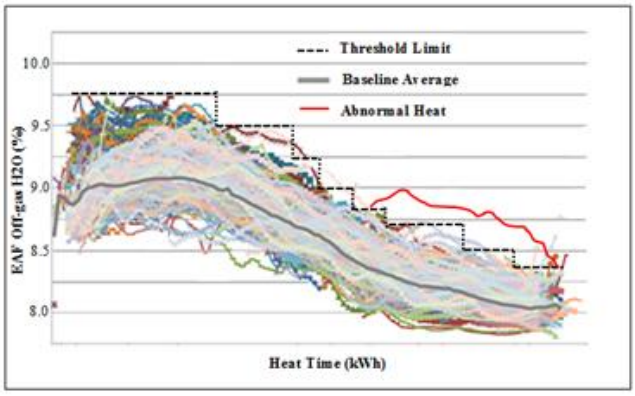

Figure 1: Baseline and Fingerprint threshold values for normal heats, and a heat with abnormal water vapor (Other curves are representatives for normal conditions in EAF).

3.2 Statistical Fingerprinting Results

Figure 2 and Figure 3 show the off-gas water vapor for Charge 1 and Charge 2 for the industrial EAF, respectively. The maximum range of variability for the off-gas water vapor is 4% for both charges. Such variability range is typically not wide, and therefore the fingerprinting method can be tested on this furnace. Moreover, the testing heats that are used to validate the model are two trial heats in which water is intentionally injected into the furnace. Figure 2 shows the off-gas water vapor, the bins, and the threshold limits for Charge 1. About 132 samples of off-gas H_2O (%) have been collected from the field in different energy clocks (kWh/Charged Ton). The two bins shown in Figure 2 are determined manually, where in each bin the water vapor dynamic is similar between the heats. The fingerprint threshold value for each bin is computed using Equations 1 and 2. In Figure 2, trial 1 heat (in red color) demonstrates a heat where water is intentionally injected into the furnace by increasing the flow rate of electrode spray by approximately 60 liters per minute from the beginning until the end of melting process. The red curve in Figure 2 is above the fingerprint threshold during the entire charge, and hence in this case this method is capable of detecting the additional injected water. Trial 2 heat (in

purple color) shows the off-gas water vapor for a heat where water is intentionally injected by increasing the electrode spray by approximately 30 liters per minute from the beginning of the Charge 1 melting until the end. The purple curve in Figure 2 pass the threshold limit slightly, and then it drops back below the limit. Hence this method is not capable of detecting trial 2 for the entire duration of charge melting. The heat time shown in Figure 2 and Figure 3 is in "kWh/Charged ton" which is the energy clock used by the EAF to pace the heat.

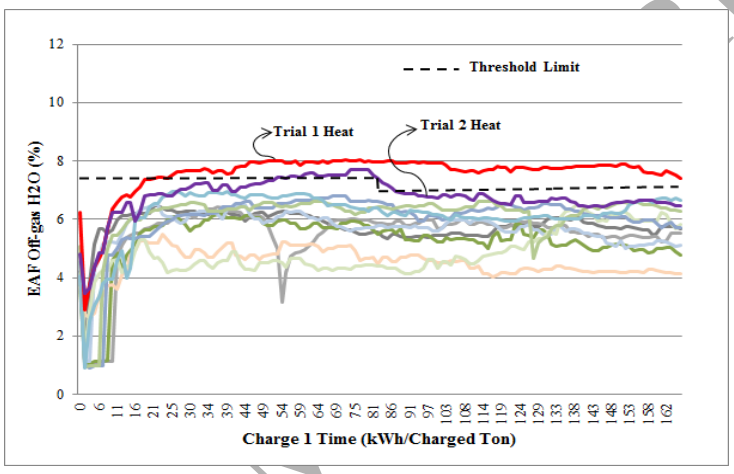

Figure 2: Fingerprinting method during Charge 1 for the industrial EAF (Other curves are representatives for normal conditions in EAF).

Similarly, Figure 3 shows 7 bins that are determined manually, where in each bin the dynamic of the water vapor measurement is similar between the heats, and the threshold value for each bin represents the upper limit to differentiate normal and abnormal operation. In addition, about 235 samples of off-gas H_2O (%) have been collected from the field in different energy clocks (kWh/Charged Ton) to plot Figure 3. Equations 1 and 2 are used to calculate the threshold limits. Trial 1 heat (in red color) in Figure 3 shows the off-gas water vapor for a heat where water is intentionally injected into the furnace by increasing the flow rate of electrode spray water by approximately 60 liters per minute during the melting process. The red curve passes through the fingerprint threshold from the beginning of the melting and drops twice below

the threshold limit. Hence the fingerprinting method can detect the additional injection in this case.

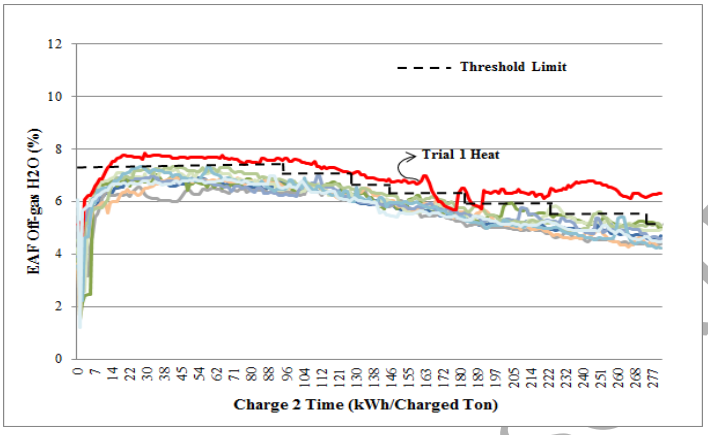

Figure 3: Fingerprinting method during Charge 2 for the EAF (Other curves are representatives for normal conditions in EAF).

Above results present that off-gas concentration measurement provides adequate information to distinguish between normal heats and heats in which significant additional water is injected into the furnace to simulate water leakage in real applications. The fingerprinting method is capable of detecting trial 1 heat where 60 liters per minute is injected, but the method is incapable of detecting the 30 liters per minute trial. In the next section, capability of machine learning methods to overcome the shortcomings of fingerprinting method is investigated. Machine learning methods explored in this work are artificial neural network and multiway projection to latent structures which use process variables to calculate expected off-gas water vapor leaving the electric arc furnace. We have also demonstrated that by applying model fusion methodology the estimation quality of off-gas water vapor can be increased.

4 Artificial Neural Network (ANN) Method

Artificial neural network (ANN) is a machine learning method that is used widely for classification and regression. ANN is utilized for classification purposes if the applied learning

technique is unsupervised and it is used for regression if the learning technique is supervised. In this paper, supervised learning is used to build the ANN model to predict EAF off-gas water vapor based on different process variables. The required steps to build the ANN model to predict the EAF off-gas water vapor are: collect and preprocess the data, create the network, configure the network, train the network, and validate the network. The learning algorithm used in this work to train the neural network is the feed forward back propagation algorithm. The selected set of heats is divided into training and testing subsets. The training heats are used to train the ANN model, and the testing heats are used to validate the generated ANN model. So, they include heats data where water is intentionally injected into the furnace to test if the ANN model can recognize the artificial additional water. The ANN method is outlined in detail in Nielsen (2015).

It should be noted that there is uncertainty in the neural network predictions due to inaccuracies in the training data and inherent limitations of the neural network model. For example, there is noise in the training data set which is constructed based on industrial real data. Therefore, a reliable measure of confidence interval is crucial in this work. The method used to construct the confidence intervals for the neural network predictions is the bootstrap method (Nielsen, 2015). This method involves creating many bootstrap samples by resampling randomly. The bootstrap estimate of the standard error is giving by (Efron and Tibshirani 1993). For this work, 10 resamples are created to estimate the standard error and then to calculate the 95% confidence interval.

4.3 Artificial Neural Network (ANN) Results

To introduce an ANN model for off-gas water vapor prediction, Matlab software has been applied. The input and output variables for the EAF are preprocessed prior to building the ANN model. The preprocessing function used in this work normalizes the input and output

variables to fall in the range of [-1, 1]; then the ANN model is constructed. The obtained ANN model is a three layer feed forward network consisting of an input layer, a hidden layer, and an output layer. The output layer has a single node because the model is used to predict one output variable (off-gas water vapor) from multiple inputs. All nodes in the input layer are connected to all nodes in the hidden layer. Similarly, all nodes in the hidden layer are connected to the node in the output layer. The input variables that are highly correlated with the off-gas water vapor are EAF total fuel flow, EAF total main oxygen Flow, EAF total injected carbon flow, off-gas CO, off-gas CO_2, off-gas O_2, EAF fume system damper position, and EAF pressure. Electrode water flow is excluded from the ANN model because the electrode flow is constant from the beginning of the heat until the end of process. By applying appropriate sensors, the values of required process variables (recognized as the model inputs and output) have been collected from the EAF. Moreover, eight nodes are used in each of the input layer and hidden layer. More nodes were tried in the hidden layer but no improvement was observed in the results. A log-sigmoid transfer function is used in the hidden layer to capture the nonlinearity of the water vapor behavior, and a linear transfer function is utilized in the output layer. The number of training heats is 15, and the number of testing heats is 9. The testing heats include 7 normal heats and 2 trial heats, where additional water is injected into the furnace from the beginning of the heat until the end. The R^2 of the ANN model built with the training heats is 90%.

Figure 4 includes two sub-figures. The left sub-figure demonstrates the ANN prediction drawn in solid line and the confidence interval in dashed line with 95% confidence level for a normal heat with three charges and a refining period. The left sub-figure shows that the ANN model provides a narrow prediction range because of the multiple layers and nodes network. The right sub-figure depicts a comparison between the measured EAF off-gas water vapor in solid

line and the off-gas water vapor predicted by the ANN model in dashed line for a normal testing heat (plotted based on about 4750 samples). There are several dips in off-gas water vapor; because whenever the operator charges the furnace with a new scrap bucket, the off-gas analyzer stops sampling and starts purging the probe and the sample line. The right sub-figure clearly shows that the predicted water vapor closely follows the measured water vapor throughout the heat.

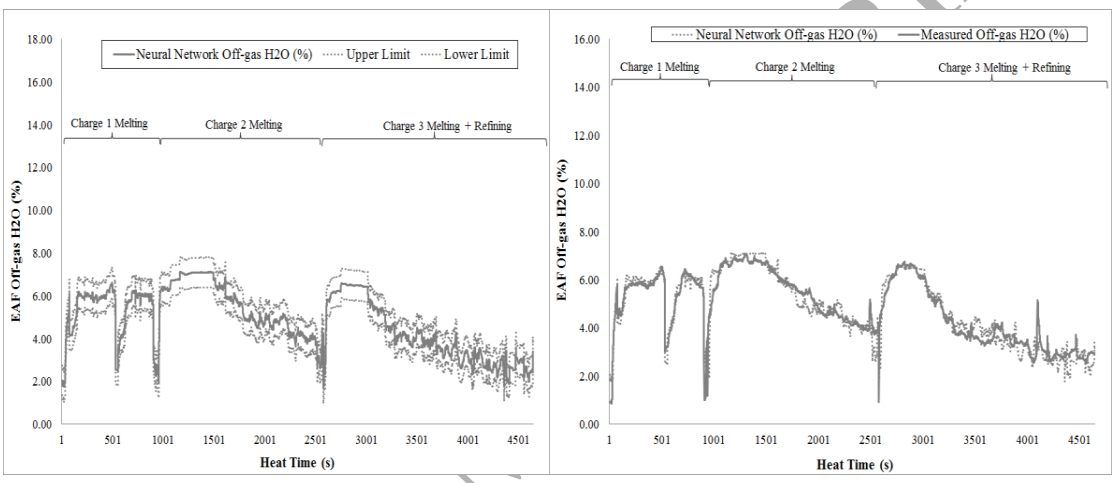

Figure 4: Left sub-figure – ANN model prediction (solid line) and the 95% confidence interval (dashed lines). Right sub-figure - Comparison between measured EAF off-gas H_2O (solid line) and ANN prediction (dashed line). Both sub-figures are for the same normal testing heat.

Figure 5 demonstrates three sub-figures. Sub-figure (a) shows the error (%) which is calculated by subtracting the calculated EAF off-gas water vapor from the measured water vapor. That figure clearly indicates that the error is below 1% for most of the heat, which implies that the predicted water vapor follows the measured water vapor with a high accuracy. Sub-figure (b) shows the histogram of errors is almost normal and approximately centered at 0. Sub-figure (c) includes normalized error histogram and also the normal distribution fitting curve, corresponding

with error/residual distribution. The mean value of the obtained normal distribution is 0.006 and the variance is 0.1556.

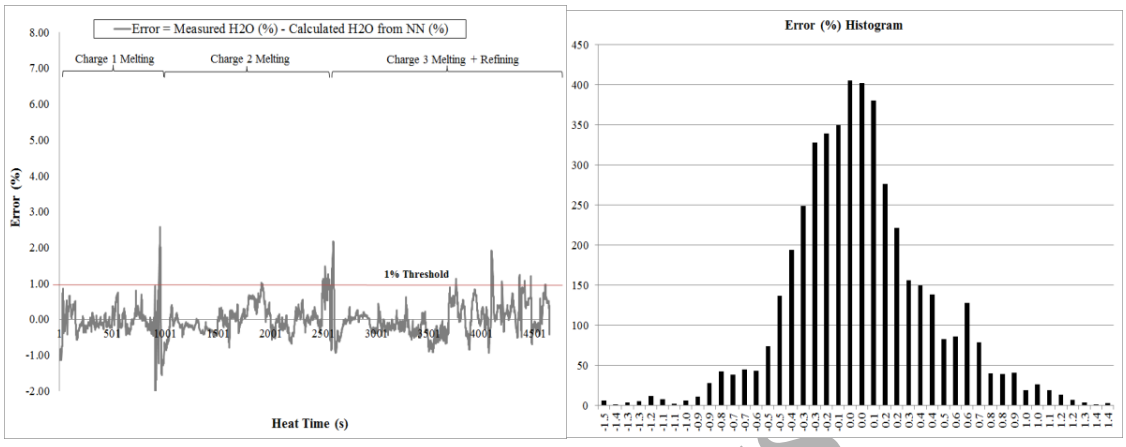

(a) (b)

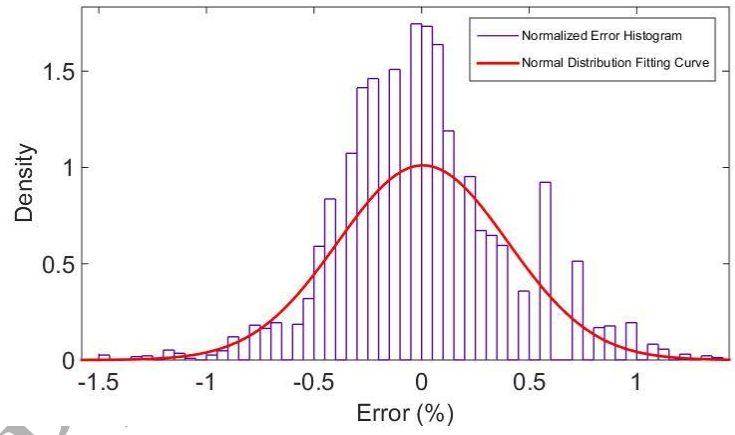

(c)

Figure 5: Sub-figure (a) - Error (%) between measured and the calculated EAF off-gas H_2O. Sub-figure (b)- Error (%) histogram. Sub-figure (c)- Normalized error histogram and normal distribution fitting curve. All sub-figures are for the same normal testing heat.

Figure 6 shows the ANN prediction in solid line and the 95% in dashed line for a trial testing heat with four charges and a refining period. The figure demonstrates that the ANN model provides a narrow prediction range because of the multiple layers and nodes network.

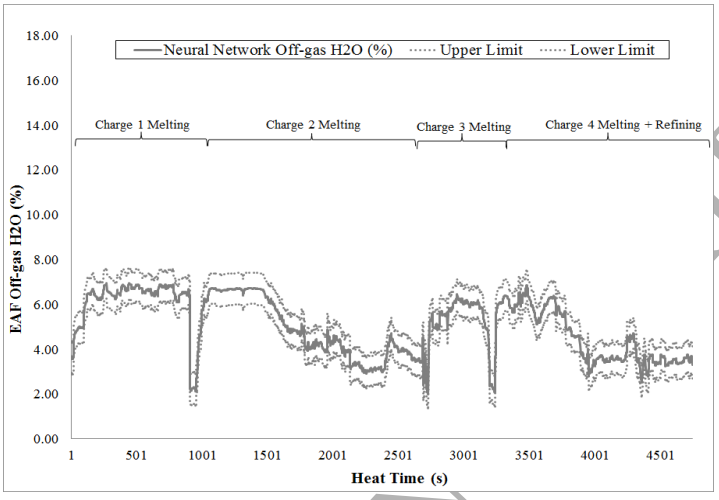

Figure 6: ANN predictions (solid line) and the 95% confidence interval (dashed line) for trial 1 testing heat.

Figure 7 includes two sub-figures for trial 1 testing heat. The left sub-figure shows a comparison between the EAF off-gas water vapor measured by the off-gas analyzer and the off-gas water vapor calculated by the ANN model. Trial 1 was conducted by increasing the electrode spray water by a total value of 60 liters per minute from the beginning of the heat until the end of the process. That sub-figure clearly implies that the measured water vapor is higher than the calculated water vapor. The right sub-figure shows the error (%) between the measured and the calculated EAF off-gas water vapor. The measured water vapor is constantly higher than the calculated water vapor because the ANN model does not include water leaks as an input to the model. In this trial, water is intentionally added into the furnace to observe if a difference can be observed between the measured and the calculated water vapor. The right sub-figure shows a continuous difference of greater than 1% between measured and predicted values from the

beginning of the heat until tapping. The error threshold is a tuning parameter, where in this case 1% is selected because it captures the water leak for both trial heats.

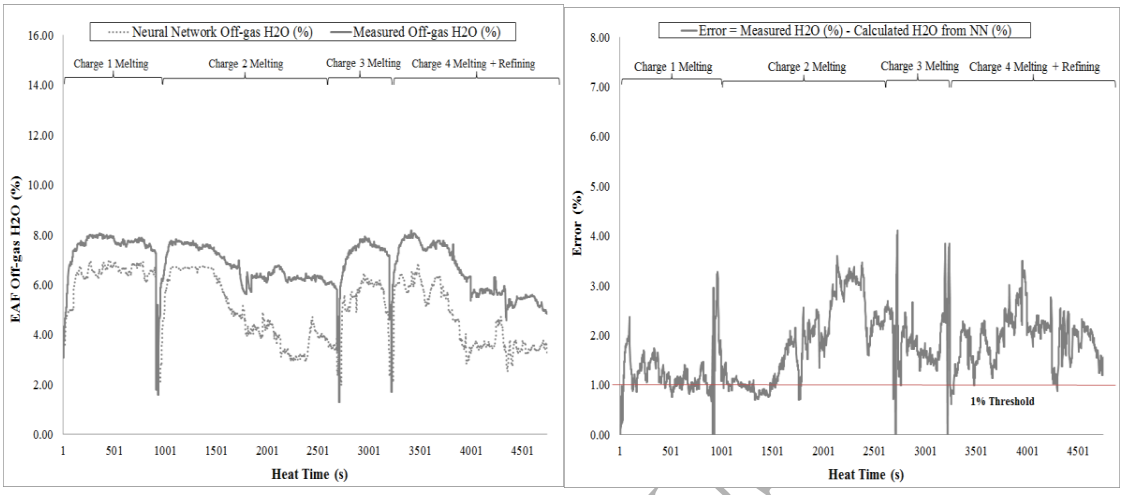

Figure 7: Left sub-figure - Comparison between measured EAF off-gas H_2O (solid line) and ANN prediction (dashed line). Right sub-figure – Error (%) between measured and the calculated EAF off-gas H_2O. Both sub-figures are for Trial 1 Testing Heat.

Figure 8 shows the ANN prediction in solid line and the 95% confidence interval level for Charge 1 of Trial 2 testing heat, where water is intentionally injected only in the first charge. Similar to Trial 1 testing heat, the figure depicts that the ANN model provides a narrow prediction range as a consequence of the multiple layers and nodes network, constructed for this model.

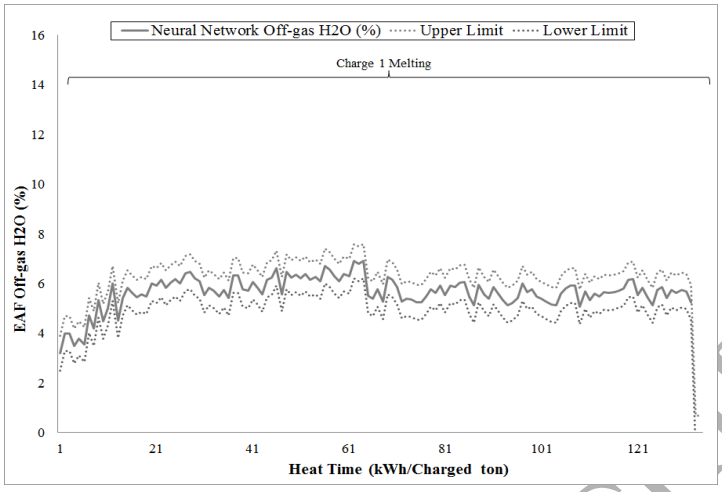

Figure 8: ANN predictions (solid line) and the 95 % confidence interval (dashed line) for trial 2 testing heat.

Figure 9 shows two sub-figures for Trial 2 testing heat. The left sub-figure demonstrates a comparison between the measured EAF off-gas water vapor and the off-gas water vapor calculated by the ANN model in percentage (%). Trial 2 testing heat is conducted by increasing the electrode spray water at a total value of 30 liters per minute during the entire first charge. The left sub-figure clearly shows that the measured water vapor is higher than the calculated water vapor. The right sub-figure shows the error between the measured and the calculated EAF off-gas water vapor. The error is above the defined 1% threshold for most of the Charge 1 melting process. However, it drops below the 1% threshold several times. Similar to Trial 1 heat, the reason that the measured water vapor is constantly higher than the calculated value is because the ANN model does not include sprayed water as an input.

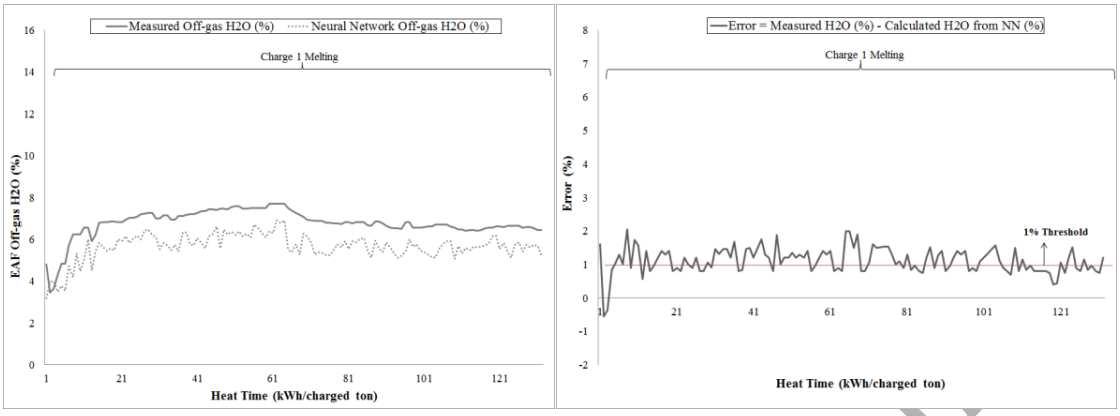

Figure 9: Left sub-figure - Comparison between measured EAF off-gas H2O (solid line) and ANN prediction (dashed line). Right sub-figure – Error (%) between measured and the calculated EAF Off-gas H_2O. Both sub-figures are for Trial 2 testing heat.

Figure 10 shows the residuals from the ANN model for the normal testing heats in the industrial EAF. This error histogram excludes the trial testing heats. The residuals shown in Figure 10 are estimates of the experimental error determined by subtracting the predicted off-gas water vapor from the measured off-gas water vapor. The figure demonstrates an error distribution that is roughly normal and is centered at approximately 0.082 with a standard deviation of about 0.47. The significant of the residuals normal distribution being centered at 0 indicates that the model error is random.

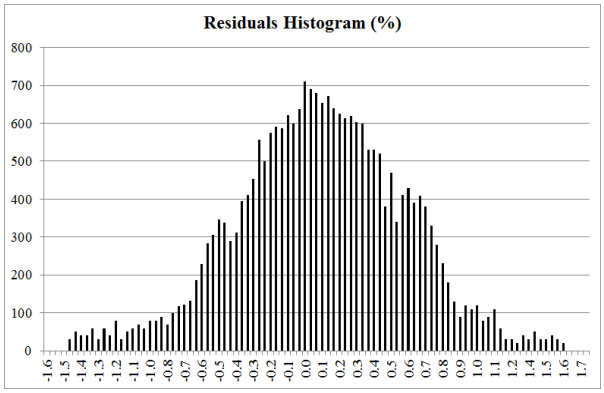

(a)

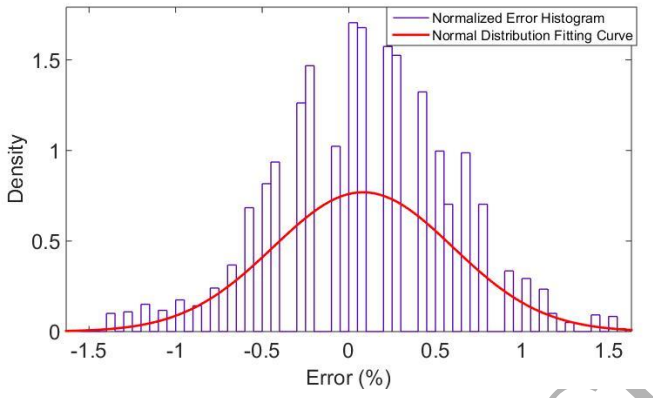

(b)

Figure 10: Sub-figure (a)-Residuals Histogram from the ANN Model for all the Normal Testing Heats. Sub-figure (b)- Normalized error histogram and normal distribution fitting curve.

5 Multiway Projection to Latent Structures (MPLS)

5.1 MPLS Method

The second machine learning method used to predict the amount of available water vapor in the furnace is multiway projection to latent structures (MPLS). As in artificial neural network, confidence intervals are necessary due to the existing noise in the industrial data; hence the bootstrap method is used to construct the 95% confidence intervals (Dunn, 2014). At this stage, 10 resamples are created to estimate the standard error and then to calculate the 95% confidence interval. The MPLS method is outlined in detail in Kourti et al. (1995).

5.2 MPLS Results

In this section, ProMV software has been applied to introduce the appropriate MPLS model for predicting off-gas water vapor. The input variables used to train the MPLS model for the industrial EAF are determined as: EAF total fuel flow, EAF total main oxygen Flow, EAF

total injected carbon flow, off-gas CO, off-gas CO2, off-gas O2, EAF fume system damper position, and EAF pressure. The number of training heats is 15 heats, and the number of testing heats is 9 heats. The testing heats include 7 normal heats and 2 trial heats where additional water is injected into the furnace from the beginning of the heat until the end of process. The numbers of principal components are 7, using cross validation. The calculated model R^2 is 78%. The first two components explain approximately 61% of the variability in the 15 heats. The remaining 5 components in the MPLS model explain approximately 17 % of the variability in the dataset.

Figure 11 includes two sub-figures. The left sub-figure shows the MPLS prediction in solid line and the confidence interval in dashed line with 95% confidence level for a normal heat with three charges and a refining period. That sub-figure depicts that the MPLS model provides a narrow prediction range. The right sub-figure shows a comparison between the EAF off-gas water vapor measured by the analyzer drawn in solid line and the MPLS off-gas water vapor prediction drawn in dashed line for a normal heat. That sub-figure indicates that the predicted water vapor follows the measured water vapor trend throughout the heat. The heat time is normalized from seconds to percentage (%).

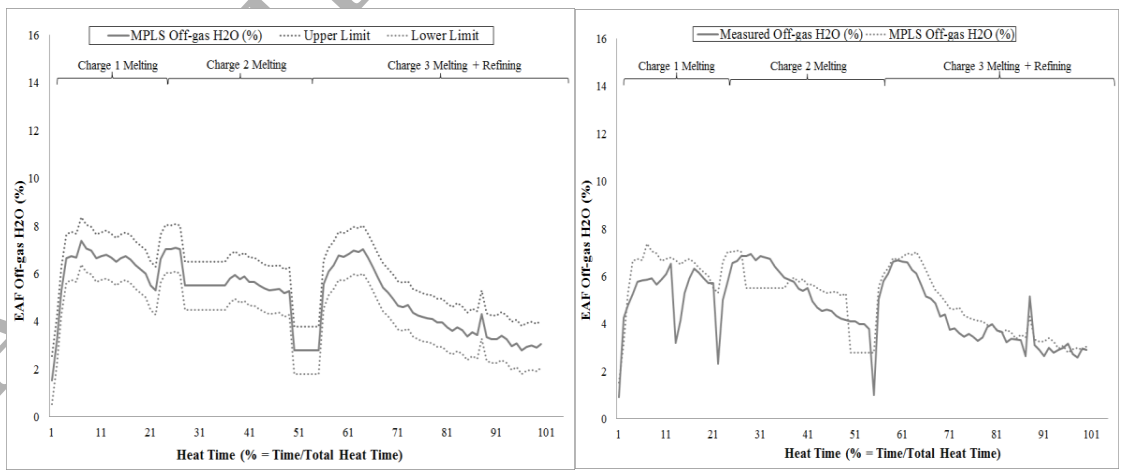

Figure 11: Left sub-figure - MPLS predictions (solid line) and the 95% confidence interval (dashed line). Right sub-figure - Comparison between measured EAF off-gas

H_2O (solid line) and MPLS prediction (dashed line). Both plots are for similar normal testing heat.

In Figure 12 the Sub-figure (a) shows the error percentage (%) which is calculated by subtracting the calculated EAF off-gas water vapor from the measured water vapor. The figure clearly depicts that the error is below the 1% threshold for most of the heat, a finding which indicates that the predicted water vapor closely follows the measured water vapor. However, in contrast to ANN model predictions, in this case there are two periods in the heat where the error is more than the 1% threshold. Sub-figure (b) shows the histogram of errors is almost normal and approximately centered at 0. Sub-figure (c) includes normalized error histogram and also the normal distribution fitting curve, corresponding with error/residual distribution. The mean value of the obtained normal distribution is -0.1 and the variance is 0.7626.

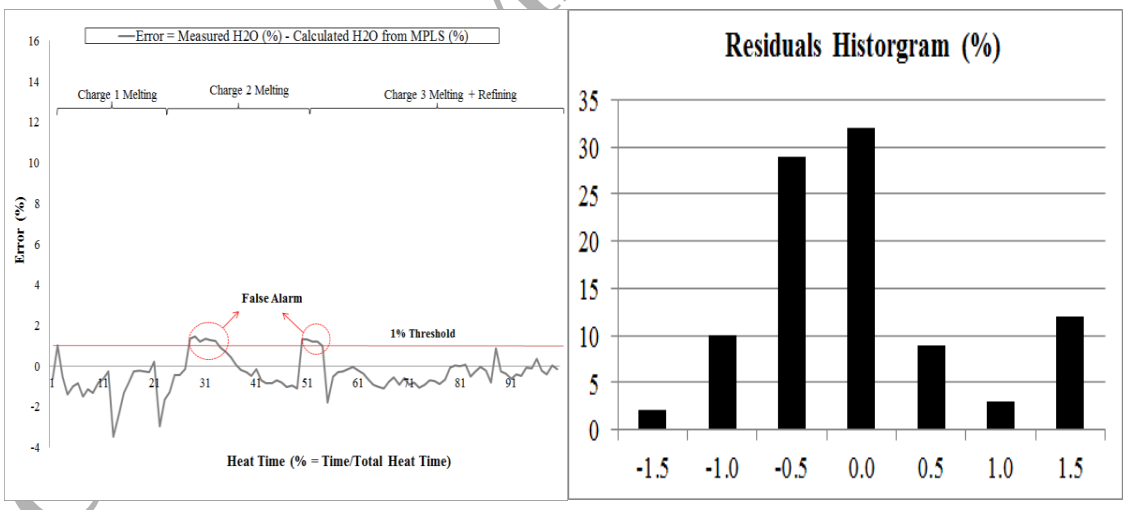

(a) (b)

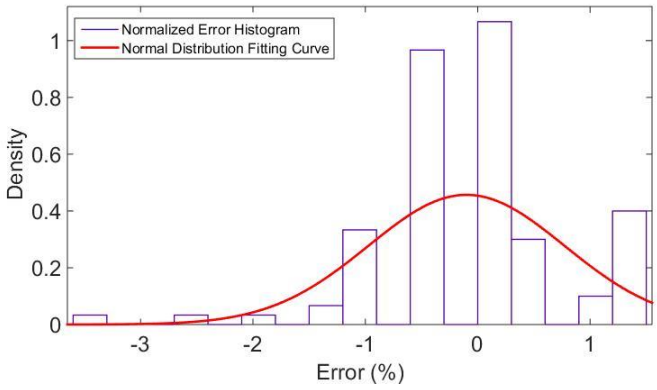

(c)

Figure 12: Sub-figure (a) – Error between measured and the calculated EAF Off-gas H_2O in percentage (%). Sub-figure (b)– Error (%) histogram. Sub-figure (c)- Normalized error histogram and normal distribution fitting curve. All sub-figures are for the same normal testing heat.

Figure 13 shows the MPLS prediction drawn in solid line and the 95% confidence interval in dashed line for Trial 1 heat with four charges and a refining period. The figure presents that the MPLS model provides a narrow prediction range.

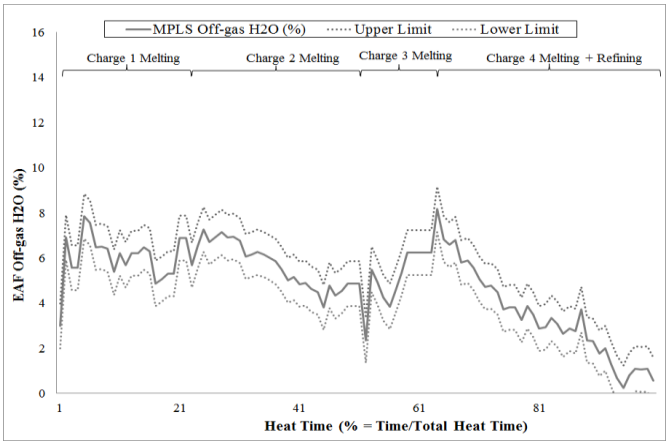

Figure 13: MPLS predictions (solid line) and the 95% confidence interval (dashed line) for Trial 1 testing heat.

Figure 14 shows two sub-figures for Trial 1 heat. The left sub-figure shows a comparison between the measured EAF off-gas water vapor and the off-gas water vapor calculated by MPLS in percentage. Trial 1 heat is conducted by increasing the electrode spray water by a total amount of 60 liters per minute throughout the heat. The left sub-figure shows that the measured water vapor is higher than the calculated water vapor for most of the heat. The right sub-figure demonstrates the error between the measured and the calculated EAF off-gas water vapor. The error is more than 1 % except in a period in the second charge where it drops below 1%.

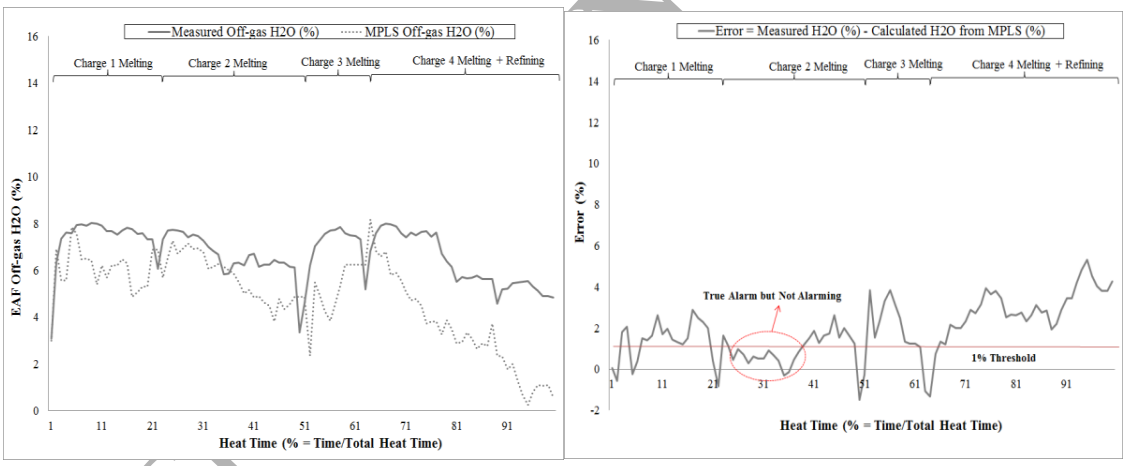

Figure 14: Left sub-figure - Comparison between measured EAF off-gas H_2O (solid line) and MPLS prediction (dashed line). Right sub-figure – Error in percentage (%) between measured and the calculated EAF off-gas H_2O. Both figures are for Trial 1 testing heat.

Figure 15 shows the MPLS prediction drawn in solid line and the confidence interval in dashed line with 95% confidence level for Trial 2 heat. The figure indicates that the MPLS model provides a narrow prediction range.

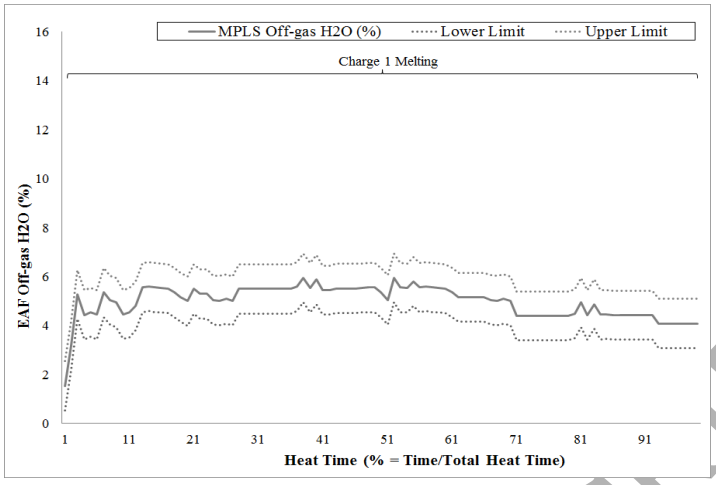

Figure 15: MPLS predictions (solid line) and the 95% confidence interval (dashed line) for Trial 2 testing heat.

Figure 16 includes two sub-figures for Trial 2 heat. The left sub-figure shows a comparison between the measured EAF off-gas water vapor and the off-gas water vapor calculated by MPLS in percentage. Trial 2 heat is conducted by increasing the electrode spray water by a total value of 30 liters per minute for the first charge. The left sub-figure clearly shows that the measured water vapor is higher than the calculated water vapor. In addition, the right sub-figure demonstrates the error in percentage (%) between the measured and the calculated EAF off-gas water vapor. As in Trial 1 heat, the reason that the measured water vapor is constantly higher than the calculated is because the MPLS model does not include water leaks or abnormal sources of water as an input to the model.

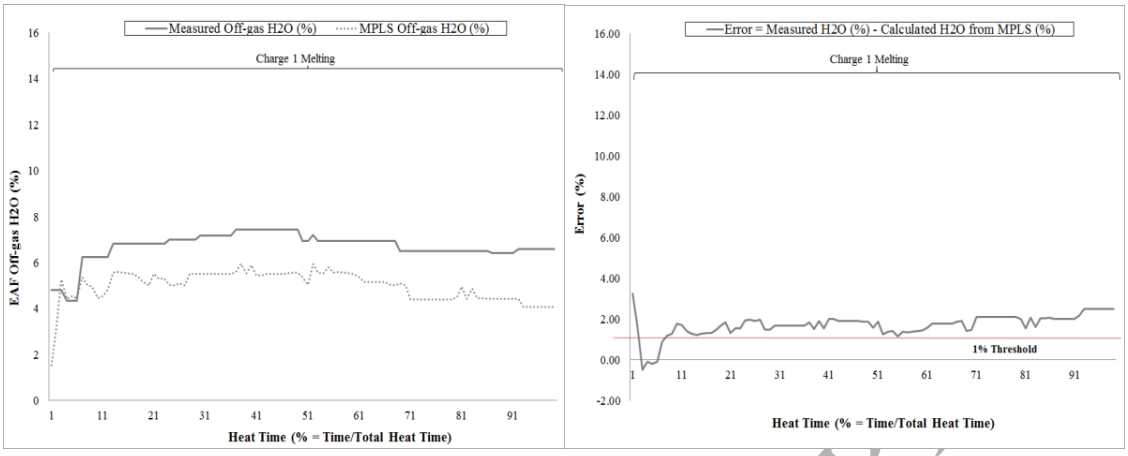

Figure 16: Left sub-figure - Comparison between measured EAF off-gas H_2O (solid line) and MPLS prediction (dashed line). Right sub-figure – Error in percentage (%) between measured and the calculated EAF off-gas H_2O. Both sub-figures are for Trial 2 testing heat.

Figure 17 shows the residuals from the MPLS model for the normal testing heats. This error histogram excludes the trial testing heats. The residuals shown in Figure 17 are estimations of the experimental errors determined by subtracting the predicted off-gas water vapor from the measured off-gas water vapor. Figure 17 shows an error distribution that is roughly normal and is centered at approximately -0.07 with a standard deviation of about 0.52. The significance of the residuals normal distribution being centered at 0 indicates that the model error is random.

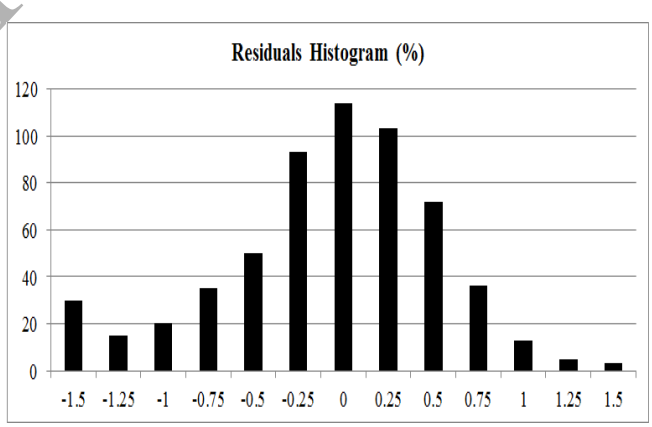

(a)

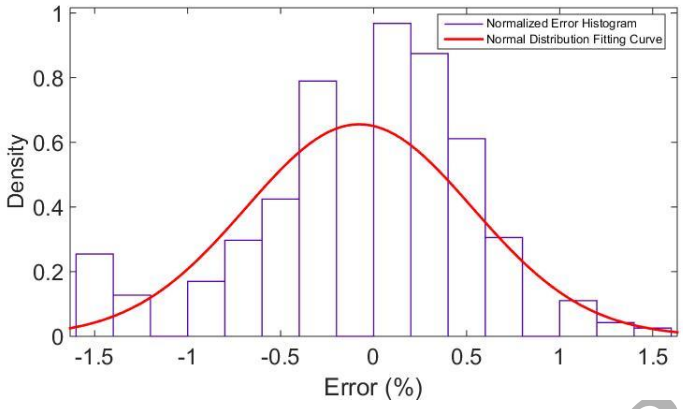

(b)

Figure 17: Sub-figure (a): Residuals Histogram from the MPLS Model for all the Normal Testing Heats. Sub-figure (b)- Normalized error histogram and normal distribution fitting curve.

6 ANN and MPLS Performance Comparison

In this paper, two machine learning techniques, multiway projection to latent structures and the artificial neural network have been used to predict the off-gas water vapor at EAF. Table 1 summarizes the obtained results for the EAF water vapor prediction performance of ANN and MPLS:

Table 1: Prediction performance comparison between ANN and MPLS.

Method	**Training Heats**	**Testing Heats**	**R^2**	**RMSEP**	**Trial Heat 1 Detection**	**Trial Heat 2 Detection**
MPLS	15	9 (7 Normal and 2 Trial Heats)	78	0.52	Partially Successful	Successful

ANN	15	9 (7 Normal and 2 Trial Heats)	90	0.47	Successful	Successful

The root mean squared prediction error (RMSEP) measures the square root of the expected squared distance between what the model predicts (y_t^p) for the water vapor and what the off-gas analyzer measures (y_t) during the heat time (t = 1 to n). RMSEP gives the standard deviation of the model prediction error and hence is an indication of the quality of the prediction. The unit for RMSEP is the same unit as the off-gas water vapor. Equation 3 shows how RMSEP is calculated:

$$RMSEP\ (\%) = \sqrt{\frac{\sum_{t=1}^{n}(y_t^p - y_t)^2}{n}} \quad (3)$$

EAF training set R^2 for the ANN model is 90% and for the MPLS model is 78%. The ANN RMSEP testing set is 0.47%, whereas MPLS RMSEP is 0.52%; hence ANN model outperformed MPLS model. Moreover, MPLS did not completely detect the additional injected water into the furnace during Trial 1. ANN model performed significantly better where the behavior of the off-gas water vapor was non-linear.

ANN is useful in the case of non-linear systems such as modeling of the EAF off-gas water vapor dynamics. ANN has the capability of capturing nonlinear and complex underlying characteristics of physical non-linear process. The method works well for large data sets, and it is a non-parametric method; thus, this fact eliminates the error in parameter estimation. Disadvantages of the ANN method include its black box nature where it is difficult to extract physical interpretation of the computed weights. In addition, the method is incapable of extrapolating the results. Another disadvantage of ANN is overfitting which occurs when the neural network memorizes the training heats but is incapable of generalizing to new heats. The

solution which has been used in this work to avoid overfitting is to collect more data and increase the size of the training set. It should be noted that although the ANN model outperformed the MPLS model, the MPLS has attractive features that the ANN lacks. MPLS model is easier to interpret and extract knowledge of the model loadings and scores. Moreover, due to the nature of the MPLS model, it can extrapolate the results. MPLS effectively handles collinearity between variables and missing data in the training and testing heats; hence the method can predict the output with acceptable precision even when some of the inputs are missing. This specification makes MPLS an appealing model for real-time predictions. However, ANN outperformed the MPLS in EAF off-gas water vapor predictions because the behavior of the off-gas water vapor is completely nonlinear.

7 Applying Model Fusion Techniques to Enhance the Prediction Accuracy

Up to this point, two independent, practical and almost accurate machine-learning-based models for estimating the value of off-gas water vapor in EAF for different operational conditions have been introduced. Nevertheless, the accuracy of the off-gas water vapor prediction can further be improved, using model fusion theory. By utilizing model fusion techniques, the outputs of available models are synergistically combined such that accuracy of predicted outputs as well as the confidence of the final inference are improved in comparison with individual models which are considered as the disparate sources of information (Khalegi et al., 2013). The general configuration of model fusion approach proposed here for predicting the value of off-gas water vapor in EAF can be observed in Figure 18.

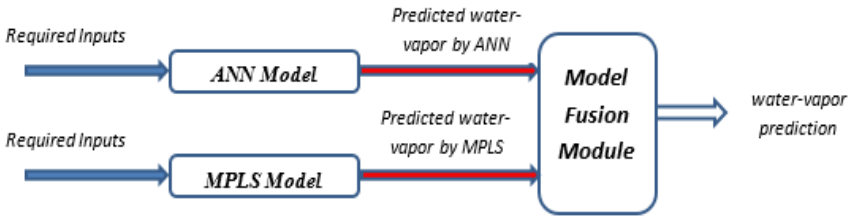

Figure 18: General Configuration of Model Fusion Technique for EAF.

One of the most popular model fusion techniques, suitable for practical and industrial applications, is Ordered Weighted Averaging (OWA) methodology. In the next subsection, a brief review about this algorithm is presented. More details are available in the cited references (Hourfar et al, 2017).

7.1 Ordered weighted averaging (OWA) operator

The first generation of OWA operator has been developed by (Yager, 1988). Generally, the OWA operator of dimension n is a mapping $OWA: R^n \rightarrow R$, which has an associated n vector $w=(w_1, w_2, \dots w_n)^T$ and the w_i are weights with the following characteristics:

$$w_i \epsilon [0,1] \text{ , } 1 \leq i \leq n,$$

$$\sum_{i=1}^{n} w_i = w_1 + \cdots + w_n = 1. \quad (4)$$

The OWA operator: $OWA(a_1, \dots, a_n) = \sum_{j=1}^{n} w_j b_j = w_1 b_1 + \cdots + w_n b_n$

where b_j is the j^{th} largest element of the set of the aggregated objects $a_1, a_2, \dots a_n$. The value of $OWA(a_1, \dots, a_n)$, determines the aggregated value of arguments. The re-ordering is the fundamental step for applying the OWA operator. OWA operator outputs are always bounded by the Max and Min operators (Brown, 2004). Moreover, the "*orness*" has been defined by (Yager, 1988) in such a way to specify the type of aggregation. By using *orness*, the analogy between the aggregation and an "*or"* operation is measured:

$$Orness(w) = \frac{1}{n-1}\sum_{i=1}^{n}(n-i)w_i \quad (5)$$

In this paper, an exponential class of OWA (Filev and Yager, 1998) has been applied. The weights in optimistic exponential OWA operator are adjusted subjected to satisfaction of a given degree of *orness*:

$$w_1 = \alpha;\ w_2 = \alpha(1-\alpha);\ldots;w_{n-1} = \alpha(1-\alpha)^{n-2};w_n = (1-\alpha)^{n-1};\quad 0 \le \alpha \le 1 \quad (6)$$

where α is related to the *orness* value correlated to the number of measurements, *n* (Afshar Khamseh et al., 2016, Hourfar et al, 2017).

7.2 Model Fusion Results:

The optimistic exponential data fusion algorithm has been implemented based on the developed EAF data-driven models, using Matlab software. The optimal fusing weights which can minimize the estimation error for two different evaluation indexes have been calculated. The selected indexes for assessing the results are Sum of Square Error (SSE) and Sum of Absolute Error (SAE). The term "error" is trivially defined as the difference between the measured off-gas water vapor value and the estimated value generated by each model. Table 2 represents the quantitative results, obtained from ANN model, MPLS model, and the fused model for a batch of test data. It can be easily observed that applying model fusion theory can enhance the performance of off-gas water vapor estimation. In other words, by utilizing the optimal fusion weights, the fused model could reduce the value of SSE and SAE about 41% and 22%, respectively, compared to the results obtained from ANN. In addition, the optimal fusing weights

for model outputs can be different based on the utilized evaluation index. A qualitative comparison between the measured data and the constructed models can be observed in Figure 19.

Table 2: Estimation evaluation for ANN, MPLS and the fusion-based model.

Type of Model	***SSE (%)***	***SAE (%)***	$W_1=W_{ANN}$	$W_2=W_{MPLS}$	***Orness=α (for n=2)***
ANN	11.94	25.61	N/A	N/A	N/A
MPLS	12.20	27.55	N/A	N/A	N/A
Fused Model #1	7.08	20.15	0.51	0.49	0.51
Fused Model #2	7.13	20.04	0.56	0.44	0.56

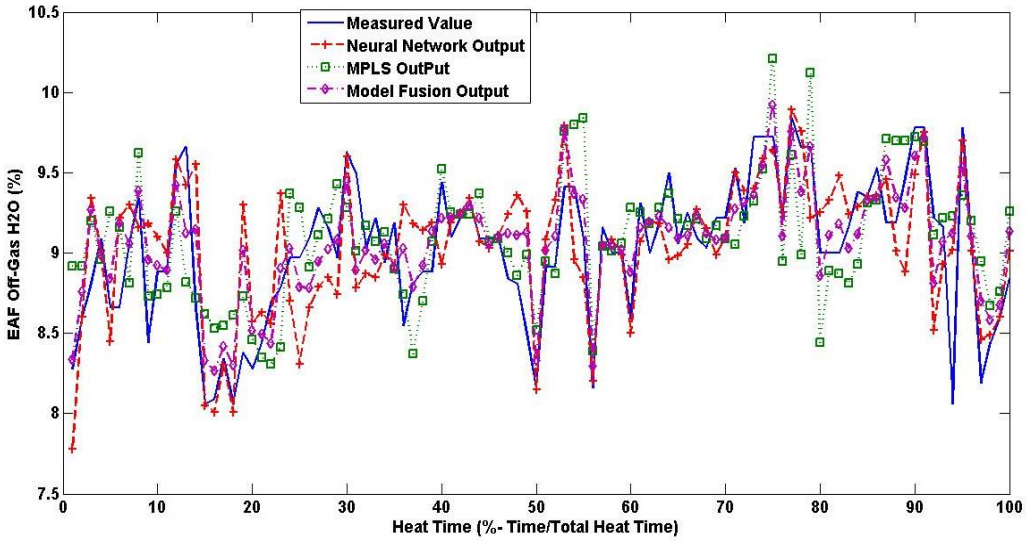

Figure 19: Comparison between real measured data and different models outputs.

8 Introduced Fault Detection Methodologies

As discussed earlier, there is always a normal level of water vapor in the freeboard off-gas inside the EAF. However, it is important to note that the absolute level of normal water

vapor in the off-gas is varying throughout the heat and from heat-to-heat depending on the quality of the scrap, burner firing rates, post combustion at any point during the heat, the level of the electrode sprays, and the level of fume system suction. To be effective, a water detection system must be able to quickly and correctly distinguish between abnormal water vapor levels due to a water leak into the EAF and a normal level of water vapor due to operating practice. In this section, two fault detection algorithms are proposed. Fault Detection Method #1 is based on the fingerprinting technique and Fault Detection Method #2 is based on using the difference between the values of measured and the predicted off-gas water vapor.

Fault Detection Method #1 is implemented when statistical fingerprinting is used. This method compares the measured off-gas water vapor value against the baseline water vapor. The baseline values are calculated based on the algorithm described earlier in section 3. Hence, this method distinguishes between "normal" and "abnormal" water vapor conditions in the EAF freeboard and then provides the operators with alerts that clearly indicate when water vapor levels exceed normal conditions. Figure 20 schematically illustrates Fault Detection Method #1 for triggering "Operator Alerts". While the method is not a failsafe method, it does provide operators with valuable real-time alerts indicating the statistical probability of excessive high amounts of off-gas water vapor in the EAF. Specific threshold limits are calculated according to the fingerprinting method described in section 3. When the off-gas water vapor is equal or less than the normal fingerprint threshold, the status is green. This indicates that the statistical probability of excessive amounts of water existence in the EAF is low. When the indicators exceed the upper threshold limit for a defined duration (e.g. 5 seconds), a "Red Alert" is issued indicating that the off-gas chemistry is significantly out of the statistically normal range and

there is a high probability of excess water in the EAF. Red Alerts require immediate protective action by EAF operating staff.

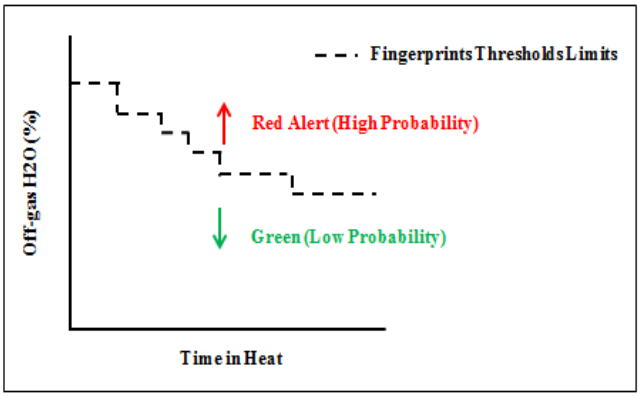

Figure 20: Operator Alerts Based on Fault Detection Method #1.

Fault Detection Method #2 is developed based on applying the introduced machine learning models (i.e. MPLS, ANN, or the combined model obtained from model fusion technique) to predict off-gas water vapor in EAF. Figure 21 schematically illustrates Fault Detection Method #2. This technique proposes to use the difference between the measured and the estimated off-gas water vapor in the furnace. Since the water vapor model considers all potential sources of water except water leak and the off-gas analyzer measures the EAF off-gas in real time; by monitoring the difference between the model and analyzers output, an indicator for water leakage can be provided. Further analysis indicates that using a 1% limit can be an acceptable alarm threshold in practice. The mentioned analysis is based on minimizing the false alarm rate and capturing the artificial leak. It should be noted that the defined threshold is a tuning parameter, where in other electric arc furnaces, this value may change. When the calculated difference exceeds 1% for 5 seconds, a “Red Alert” is activated to indicate that there

is excessive water in the furnace. The 5 seconds timer, which may vary in different EAF, is also a tuning parameter to minimize false alarm rate and capture the artificial leak.

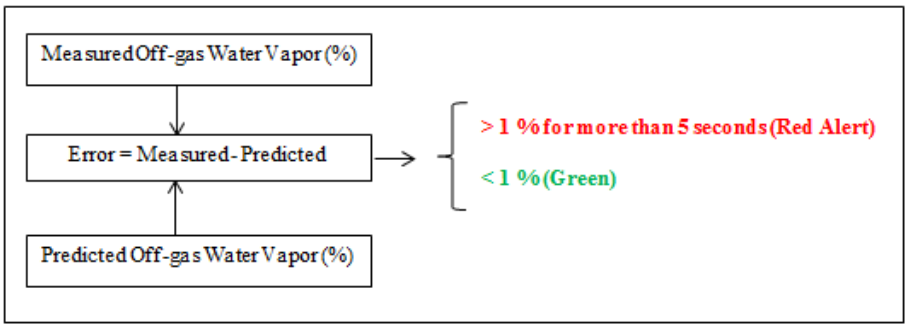

Figure 21: Operator Alerts Based on Fault Detection Method #2

10 Conclusions

Different empirical predictive models to predict the amount of off-gas water vapor have been developed and tested on an industrial electric arc furnace. The studied models are statistical fingerprinting, artificial neural network, multiway projection to latent structures, and also the obtained model from the fusion of ANN and MPLS. Robustness issues related to each method are discussed in detail and a performance comparison between the methods is presented. This paper also investigates feasibility of applying model fusion theory to improve the performance of the prediction of the off-gas water vapor. Two fault detection methods are also proposed in this paper. Fault detection method #1 has been designed using statistical fingerprinting and Fault detection method #2 has been developed based on machine learning modeling techniques. Opportunities for future work include increasing the quantity of available measurements that would improve the performance of the off-gas water vapor predictive models. For example, measuring scrap and DRI composition and off-gas temperature can improve the accuracy of the empirical predictive models. Another interesting problem would be to develop a water detection method based on off-gas hydrogen monitoring. The water shift reaction produces less off-gas

hydrogen as the temperature rises in the furnace, but the reaction can produce hydrogen at low temperatures in the furnace. The objective of looking at this problem is to see if off-gas hydrogen contains water leak information that can improve the performance of the water detection framework to detect smaller leaks in the furnace (i.e. below 30 liters/min leaks).

References

Khamseh, A. S., K. Sedigh, A., B. Moshiri, A. Fatehi, "Control performance assessment based on sensor fusion techniques," *Control Engineering Practice*, **49**, 14 (2016).

Alshawarghi, H., *Water Detection Framework for Industrial Electric Arc Furnaces*, University of Waterloo, Dept. of Chemical Engineering (2016).

Bano, G., P. Facco, F. Bezzo, M. Barolo., "Probabilistic Design space determination in pharmaceutical product development: A Bayesian/latent variable approach," *AIChE J.*, **64**, 2438 (2018).

Brown, R. G., *Smoothing, forecasting and prediction of discrete time series*, Mineola, New-York: Dover publications inc. (2004).

Chetouani, Y., "A Neural Network Approach for the Real-time Detection of Faults," *Empirical Environmental Research and Risk Assessment*, **22**, 339 (2008).

Dunn, K., *Process Improvement Using Data*. McMaster University, Hamilton, ON (2014).

Efron B., and R. J. Tibshirani., *An Introduction to the Bootstrap*, Chapman and Hall, London, UK, (1993).

Filev, D. and R. Yager, "On the issue of obtaining OWA operator weights," *Fuzzy Sets and Systems*, **94**, 157 (1998).

Freeman, P., R. Pandita, N. Srivastava, and G. J. Balas, "Model-Based and Data-Driven Fault Detection Performance for a Small UAV", *IEEE/ASME Transactions on Mechatronics*, **18**, 1300 (2013).

Fruehan, R. J., "The Making, Shaping and Treating of Steel", *AISE Steel Foundation*, Pittsburgh, PA, 1998.

Grieshaber, K. and F. Martinez. "ZoloSCAN Laser Diagnostic System for EAF Leak Detection and Process Optimization." Proceedings of Metec Conference, Dusseldorf, Germany, June 15–19, 2015.

Hourfar, F., B. Moshiri, K. Salahshoor, and A. Elkamel, "Real-time Management of the Waterflooding Process Using Proxy Reservoir Modeling and Data Fusion Theory," *Comp. and Chem. Eng*, **106**, 339 (2017).

Irons, G. A., "Developments in Electric Furnace Steelmaking", *AISTech Conference*, Charlotte, NC (2005).

Isermann, R., "Fault Diagnosis of Diesel Engines,"*Mechanical Engineering*, **135**, 6 (2013).

Jones, J.A.T., E. Pretorius, and H. Oltmann, *EAF Fundamentals, Notes by Process Technology Group at LWB Refractories and Nupro Corporation* (2005).

Jones, J.A.T., "Electric Arc Furnace Design and Operations," *AISE Electric Furnace Steelmaking Seminar*, Birmingham, AL (2014).

Khaleghi, B., A. Khamis, F. O. Karray, and S. N. Razavi, "Multisensor data fusion: a review of the state-of-the-art," *Information Fusion*, **14**, 28 (2013).Kourti, T. and J. F. MacGregor, "Multivariate SPC Methods for Process and Product Monitoring," *Journal of Quality Technology*, **28**, 409 (1996).

Kourti, T., P. Nomikos, and J. F. MacGregor, "Analysis, Monitoring and Fault Diagnosis of Batch Processes Using Multiblock and Multiway PLS," *Journal of Process Control*, **5**, 277, (1995).

Li, B., F. Zhou, H. Li, A. Duguid, L. Que, Y. Xue, and Y. Tan, "Prediction of CO2 leakage risk for wells in carbon sequestration fields with an optimal artificial neural network." *International Journal of Greenhouse Gas Control*, **68**, pp. 276-286, 2018.

Lin, Ming-I, W. Groves, A. Freivalds, E. Lee, and M. Harper, "Comparison of artificial neural network (ANN) and partial least squares (PLS) regression models for predicting respiratory ventilation: an exploratory study," *European Journal of Applied Physiology*, **112**, 1603 (2012).

Macgregor, J.F. and P. Nomikos, "Monitoring Batch Processes Using Multiway Principal Component Analysis," *AIChE J.*, **40**, 1361 (1994).

Macgregor, J. F., C. M. Jaeckle, C. Kiparissides, and M. Koutoudi, "Process Monitoring and Diagnosis by Multiblock PLS Methods." *AIChE J.*, **40**, 826 (1994).

Mathworks, *Neural Network Toolbox User's Guide for Use with MATLAB* (2014).

Meng, M. and G.A. Irons, "Comparison of Electric Arc Models with Industrial Data," *58th Electric Furnace Conference and 17th Technology Conference, ISS Publishers*, Warrendale, PA, 183 (2000).

Nielsen, Michael, *Neural Networks and Deep Learning*. Determination Press (2015).

Nomikos, P., "Detection and Diagnosis of Abnormal Batch Operations Based on Multi-Way Principal Component Analysis," *ISA Transactions*, **35**, 259 (1996).

Nomikos, P. and J. F. MacGregor, "Multi-Way Partial Least Squares in Monitoring Batch Processes," *Chemometrics and Intell. Lab. Sys.*, **30**, 97 (1995a).

Quiroga, P., "Leaks Prevention: Design Directives to Achieve Reliable Water Cooled Equipment," *Maintenance Guild Presentation*, Beaver Falls, PA (2013).

Rashid, M., P. Mhaskar* and C.L.E. Swartz, ``Handling Multi-rate and Missing Data in Variable Duration Economic Model Predictive Control of Batch Processes with Application to Electric Arc Furnace Operation," *AIChE J.*, in press.

Rashid, M., P. Mhaskar* and C.L.E. Swartz, ``Multi-rate Modeling and Economic Model Predictive Control of the Electric Arc Furnace,'' *J. Proc. Cont.*, **40**, 995 (2016).

Sheibat-Othman N., N. Laouti, J. Valour, and S. Othman, "Support Vector Machines Combined to Observers for Fault Diagnosis in Chemical Reactors." *Can. J. of Chem. Eng.*, **92**, 685 (2014).

Yager, R. R., On ordered weighted averaging aggregation operators in multicriteria decision making," *IEEE Transactions on Systems, Man and Cybernetics*, **18**, 183 (1988).

Yu, J. A., "A Bayesian inference based two-stage support vector regression framework for soft sensor development in batch bioprocesses," *Comp. and Chem. Eng.*, **41**, 134 (2012).

Zuliani, D.J., H. Alshawarghi, V. Scipolo, M. Khan, and W. Biliski, "Real-Time Water Detection Technology at ArcelorMittal Coatesville," *Iron & Steel Technology*, 3340 (2014).